19th Australasian Fluid Mechanics Conference
Melbourne, Australia
8-11 December 2014

DNS of an Airfoil at Angle of Attack with an Elastic Trailing-Edge Extension

S. C. Schlanderer[1] **and R. D. Sandberg**[1]

[1]Aerodynamics and Flight Mechanics Research Group,
University of Southampton, Southampton SO17 1BJ, United Kingdom

Abstract

A framework to conduct Direct Numerical Simulations of flows around airfoils with elastic trailing-edge extensions was developed. To that end a well-validated compressible DNS-code was coupled to a newly implemented structural solver. The moving body is represented by a novel boundary data immersion method originally developed for incompressible flows and extended to compressible flows for the current work. It is demonstrated that this method is capable of representing near-wall fluid and thermodynamic fluctuations accurately. In addition the simulation of an oscillating cylinder shows that the noise generated by a moving body represented with the boundary data immersion method matches the analytical solution closely. Finally initial results of a flow around an airfoil with a flexible trailing-edge extension are presented.

Introduction

Trailing-edge (TE) noise is a dominant contributor to noise produced in many engineering applications featuring flows around lifting surfaces such as wings and rotating blades. Recent analytical studies of vibro-acoustic systems by Manela [8] and Jaworski & Peake [3] conclude that the body motion of an airfoil or a TE does influence the characteristics of the scattered noise. Depending on the structural parameters and the frequency the noise level can vary significantly. This behaviour was confirmed by the first DNS of an elastic TE in our previous study[10]. The results from simulations of two laminar boundary layers that are divided by a flat plate indicate a noise reduction of an elastic plate compared to a rigid one. The noise reduction can be observed in the upstream direction only and depends on the frequency. For frequencies close to the natural frequencies of the elastic plate the noise level is higher than in the rigid case. The main noise reduction occurs in the low frequency range away from the natural frequencies of the structure. Better knowledge of the fluid-structure interaction and its effect on the scattered noise can lead to more silent airfoil and blade designs. Therefore the present study aims to deepen the understanding in this field by conducting direct numerical simulations (DNS) of flows around elastic trailing-edges. To that end a well validated in-house compressible DNS code is used to directly calculate the near-field hydrodynamics and the far-field sound. The numerical method of the structural solver and the method to represent the moving body used in [10] imposed severe timestep restrictions and showed unfavourable behaviour on curvilinear grids. Therefore new methods had to be implemented and developed which are described and validated in this paper. Finally the fluid-structure interaction framework was used to conduct the first DNS of a flow around an airfoil at an angle of attack of 5° and Reynolds number based on the chord of $Re = 5 \times 10^4$ with a flexible flat plate extension attached to the TE.

Governing Equations and Numerical Methods

Structure

The structure is modelled as a bending beam that is clamped at one side and has a constant cross section with uniform material properties. Furthermore it is assumed that the impact of the fluid on the solid structure is given by the pressure difference between upper and lower side of the plate and leads to small deflections only. The equation of motion for the structure can be modelled by the Euler-Bernoulli beam equation for the structure deflection w_s and velocity v_s and written as a system of two first order differential equations with

$$\frac{\partial w_s}{\partial t} = v_s \tag{1a}$$

$$\frac{\partial v_s}{\partial t} = \frac{1}{\rho_s A}\left(\Delta p - EI\frac{\partial^4 w_s}{\partial s^4}\right) \quad . \tag{1b}$$

Here ρ_s denotes the structural density, A is the cross section of the beam and Δp the line load from the pressure difference. Furthermore EI is the bending rigidity with Young's modulus E and the second moment of inertia of the cross section $I = h^3\, d/12$ with the height h and depth d of the structure. Dimensionless quantities are obtained by nondimensionalizing with the reference fluid density and velocity, or a combination thereof.
The implemented structural solver first calculates the right hand side of equation (1b) using the pressure load from the fluid simulation and the spatial derivative of the deflection. The solution is advanced in time by a fourth order accurate ultra low storage Runge-Kutta scheme that is also employed in the fluid solver. The spatial discretization to calculate $\frac{\partial^4 w}{\partial x^4}$ is achieved with a fourth order accurate compact finite difference scheme [6]. The fourth derivative of the deflection is calculated recursively. In order to suppress spurious oscillations a wave number optimised filtering routine is employed after each Runge-Kutta stage and after taking the derivative [5].
The coupling to the fluid solver is achieved at the beginning of each time step by updating the pressure values. The position and velocity of the structure are updated once at the end of each timestep. Since the timestep is small in order to capture the relevant time scales of the fluid motion the influence of the discrepancy in time are negligible.

Fluid

A detailed description of the DNS-code and the applied methods can be found in [10]. The focus in this section is on the method that is employed to represent moving bodies in aeroacoustic simulations. To that end a Boundary Data Immersion Method (BDIM) newly developed for incompressible flows by Maertens & Weymouth [7] is extended to be used in compressible flows. The BDIM allows smooth coupling between a solid body subdomain Ω_s and a compressible fluid subdomain Ω_f to obtain a meta equation that is valid in the whole domain under consideration. In this method the solid body domain does not need to coincide with the background grid. The general formulation for a meta equation of an arbitrary field variable Φ is

$$\Phi_M(\vec{x},t) = \begin{cases} \Phi = b & ,\text{for } \vec{x} \in \Omega_b \\ \Phi = f & ,\text{for } \vec{x} \in \Omega_f \end{cases} \quad , \tag{2}$$

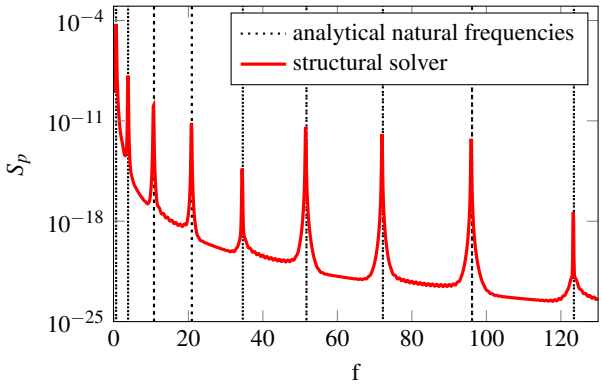

Figure 1. Comparison of natural frequencies obtained from the structural solver compared to the analytical solution.

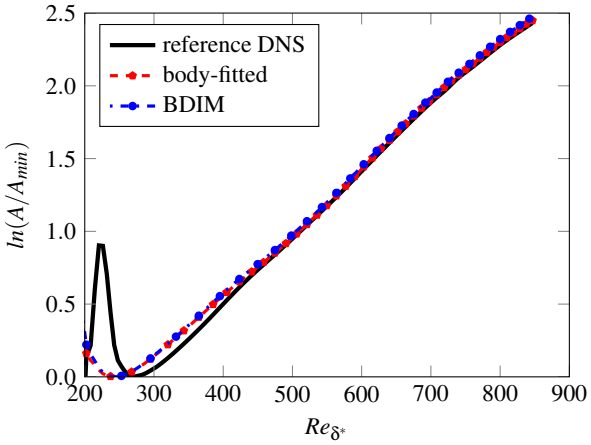

Figure 2. Amplitude growth rate of streamwise velocity disturbance as a function of the streamwise position comparing data from Husmeier [2] with simulations using the BDIM and body-fitted boundary conditions.

where b and f are the governing equations for the body and fluid subdomain, respectively. Both subdomains can then be smoothly coupled with an interpolation function that acts in a smoothing region of size ε where both domains overlap. The two functions depend on d only which is the signed distance from the surface. Values with $d < 0$ refer to the inside and $d > 0$ to the outside of the solid body. The final equation that is implemented into the code and used to map the velocity and temperature field between both subdomains is

$$\begin{aligned}\Phi_\varepsilon = f(\Phi,\vec{x},t)\mu_0^\varepsilon + b(\Phi,\vec{x},t)\left(1-\mu_0^\varepsilon\right) \\ +\mu_1^\varepsilon \frac{\partial}{\partial n}\left(f(\Phi,\vec{x},t) - b(\Phi,\vec{x},t)\right) \quad .\end{aligned} \tag{3}$$

For more details on the concept of the BDIM, the derivation of the second order accurate coupling between both domains and the exact expressions for $\mu_0^\varepsilon(d)$ and $\mu_1^\varepsilon(d)$ please refer to reference [7].

Validation

Structure

The newly implemented model is validated with the response to an initial pulse of pressure loading acting on the beam. The free vibrations that follow the initial excitation are then sampled. In the postprocessing the time history of the deflection at the free end is then converted to a power density spectrum. The analytical natural frequencies can be calculated with

$$f_j = \frac{\lambda_j}{2\pi L^2}\sqrt{\frac{EI}{\rho_s A}} \quad , \tag{4}$$

with $\lambda_1 = 1.875$ and $\lambda_j = (2j-1)\pi/2$ for $j = 2,3,4,...$[11]. Figure 1 compares the spectral power density obtained from a simulation with an initial pulse of pressure loading to the analytically calculated natural frequencies. The overall agreement for the first nine modes is very good. In the coupled simulations the excitation frequency from the pressure loading will be within the range of the first three natural frequencies. Hence the results show that the implemented model is suitable to represent an elastic TE extension in a fluid-structure interaction simulation.

Fluid - Oblique Wave Growth in Supersonic Boundary Layer

When TE noise is considered a very accurate representation of the near-wall flow and thermodynamics is crucial. This is attributed to the fact that fluctuations in the boundary layer are the "input" of the TE noise scattering mechanism. Furthermore a correct thermodynamic behaviour is crucial since the noise is calculated directly from the compressible Navier–Stokes equations. In order to evaluate these properties of the BDIM the growth of oblique waves in a supersonic flat plate boundary layer was chosen as a rigorous and challenging validation case. Oblique waves are a three dimensional instability mechanism in supersonic boundary layers that are relevant for transition in low disturbance environments [9]. The flow that is considered is a supersonic flat plate boundary layer at $Ma = 3.0$ and $Re = 1578102$. The instabilities are triggered by disturbing the flow close to the wall at $(x,y) = (0.02, 0.0003)$ with sinusoidal momentum forcing. The forcing amplitude is $A = 1.0 \times 10^{-3}$ and the frequency is $f = 12.558136$. At the inflow a Blasius boundary layer profile with a Reynolds number based on displacement thickness of $Re_{\delta^*} = 273$ is prescribed. At the freestream and outflow boundary a non-reflective characteristic boundary condition was applied.

For the body-fitted reference case a rectangular Cartesian grid with $1.59172 \times 10^{-3} < x < 0.45598$ and $0.0 < y < 4.70223 \times 10^{-2}$ was employed. In the streamwise direction the 281 grid points are distributed equidistantly with $\Delta x = 1.623 \times 10^{-3}$ over the whole domain. In the wall normal direction the grid spacing stretches from $\Delta y = 3.51 \times 10^{-5}$ at the wall to $\Delta y = 1.644 \times 10^{-3}$ at the freestream boundary. The spanwise direction is discretized with a spectral method using two Fourier modes spanning over $\Delta z = 0.0299817$. In the validation case where the BDIM represents the wall boundary condition, 100 grid points were mirrored in the wall normal direction. The surface of the body that was represented by the BDIM was placed between the first and second point of the original grid. The void below the original position of the wall was initialized with zero velocity and uniform density and temperature. The wall represented by the BDIM had a finite thickness of 4.216×10^{-4}.

After the initial transient snapshots of the flow field were gathered for two forcing cycles. From the Fourier transform of the streamwise velocity component the maximum amplitude at each streamwise location was determined and then normalized by the lowest amplitude of all streamwise positions. Figure 2 compares the results obtained with the BDIM with data using body-fitted boundary conditions and the reference [2]. It can be appreciated that the BDIM reproduces the growth rates very accurately. The inital deviations between the reference and the present code is due to the fact that the forcing was done differently. This result shows that the BDIM is capable

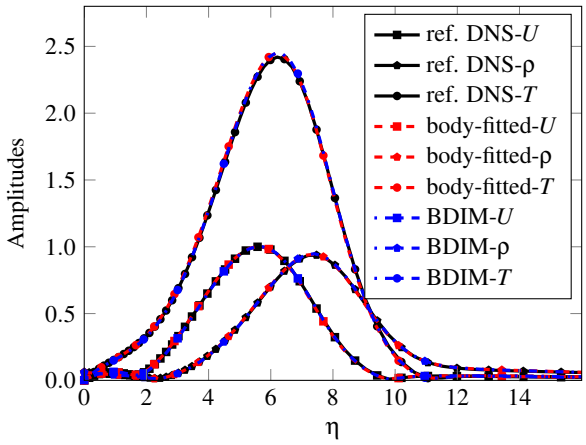

Figure 3. Amplitude distribution of streamwise velocity U, density ρ and temperature T in wall-normal direction at $Re_x = 700$ from simulations using the BDIM in comparison to simulations with body-fitted boundary conditions and the reference [2].

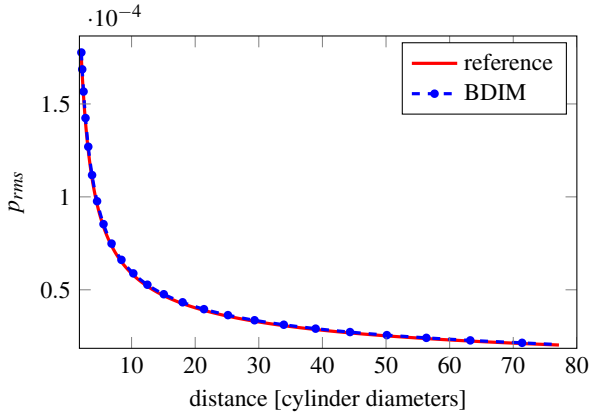

Figure 4. Comparison of pressure fluctuations over distance from center of cylinder in the direction of the body motion between analytical solution and simulations using the BDIM

of accurately representing highly sensitive instability growth adjacent to a wall boundary in a three dimensional flow.

In addition to the instability growth rate, the fluctuation amplitudes are evaluated in figure 3 as a function of the normalized wall distance at $Re_{\delta^*} = 700$. The amplitudes are normalized by the maximum velocity amplitude. The velocity amplitude profile proves that the very good agreement between the BDIM and the references is not limited to the maximum amplitude at a streamwise position as presented before. It also matches the shape of the profile along the wall normal direction perfectly. Furthermore the fluctuations of the thermodynamic quantities density ρ and temperature T are computed very accurately. In addition the normalization that was chosen shows that density fluctuations are almost as high as the velocity fluctuations and the temperature fluctuations are a factor of ≈ 2.4 higher than the velocity fluctuations, thus underlining the importance of a good representation of the near wall thermodynamics for that case. Representing these quantities accurately will be necessary when the noise generation at a TE is considered.

Fluid - Noise from oscillating Cylinder

This section focusses on the BDIM's capability to represent the acoustic noise generation of a moving body which is demonstrated by the simulation of a transversely oscillating cylinder in a medium at rest. The cylinder is considered to have an infinite extension in the spanwise direction, hence the problem can be considered to be 2D.

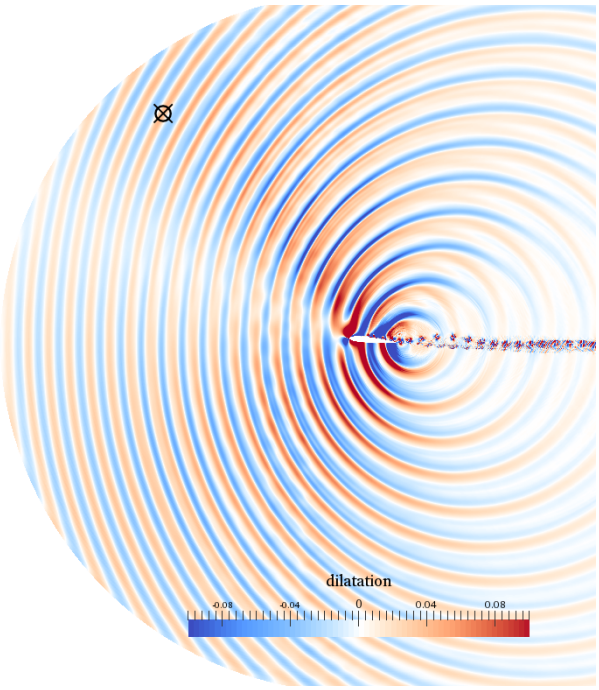

Figure 5. Contours of dilatation showing the acoustic field of the simulation with the flexible TE extension.

The cylinder's diameter d_{cyl} was set to unity and the vibration amplitude was 5% of the diameter and the vibration velocity amplitude $v_{vib} = 0.0094$. With $Ma = 1$ these parameters result in an acoustic wave length of $\lambda = 33.3 d_{cyl}$. The cylinder was discretized with 160 equispaced grid points per diameter and surrounded by another $1.25 d_{cyl}$ of equispaced grid in each direction. For the far-field the grid is then stretched over 200 grid points to a resolution of 20 grid points per acoustic wave length. In order to avoid any reflections from the boundaries around the acoustic far field another 40 grid points were appended in each direction with strong grid stretching.

The analytical solution for the pressure fluctuations p_{rms} of this radiation problem is

$$p_{rms} = Re\left\{\left| -j\rho_0 v_{vib} cos(\theta) \frac{H_1^{(2)}(kr)}{Ma H_1^{(2)'}(ka)} e^{j\omega_{vib}t} \right|\right\} \quad , \quad (5)$$

where $H_1^{(2)}$ is a Hankel function of the second kind and first order and $H_1^{(2)'}$ its derivative. Furthermore ρ_0 is the mean density of the medium at rest [1]. Figure 4 compares a p_{rms} profile from a simulation using the BDIM with the analytical solution. The data was extracted along the radial direction aligned whith the cylinder's motion. The results from the simulation show excellent agreement with the analytical solution in the near and the acoustic far field. This demonstrates that the BDIM is an appropriate method to perform direct noise simulations featuring moving bodies.

Airfoil with Elastic Trailing-Edge Extension

In the final set of simulations the BDIM was used to simulate a flexible TE extension of a NACA0012 airfoil profile at an angle of attack (AoA) $\alpha = 5°$. The chord based Reynolds-Number was $Re_c = 5 \times 10^4$ and the inlet Mach-Number $Ma = 0.4$. The airfoil is discretized with a two block C-mesh where one block wraps around the airfoil and the second covers the wake region.

	grid points	Length	Structural parameters	
foil normal	692	7.2	Length L	0.101
foil tangential	1066	≈ 2	height $h_s * 10^3$	1.637
wake streamw.	752	5.98	Density ρ_s	1529
wake pitchw.	1383	14.4	Youngs – Modulus E	837122

Table 1. Grid and domain dimensions and structural parameters. All dimensions are normalized with the chord length C. The structural parameters are non-dimensionalized with fluid quantities from the free-stream or combinations thereof.

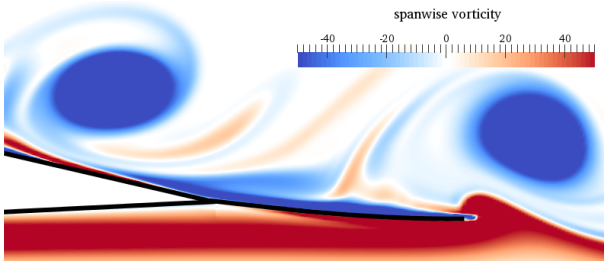

Figure 6. Contours of spanwise vorticity showing the flexible TE extension in a deflected state.

The grid was derived from grid G3 used in Jones et al.[4] where its resolution was determined using an iterative approach. The number of grid points and the domain's dimension are listed in table 1. For further details on the mesh please refer to [4]. In addition table 1 presents the structural parameters for the elastic TE extension. The extension was discretized with 30 equispaced grid points for the structural solver.
Figure 5 shows the dilatation contours at an arbitrary instant of time. It shows a very clean acoustic field where the noise mainly originates from the trailing-edge and is scattered upstream. The vortices that are shed from the laminar separation bubble can be clearly identified in figure 6 which shows instantaneous spanwise vorticity contours at the aft of the airfoil. The coherent vortex shedding leads to strong pressure disturbances that drive the motion of the elastic TE extension. The deflection of the extension with the shape of bending mode two can be found when the plot is examined carefully.
The power spectral density of the pressure time signal is presented in figure 7 and allows an initial statistical evaluation of the acoustic field. The vortex shedding frequency and its first harmonic can be clearly seen at $f \approx 3.5$ and $f \approx 7$ respectively. In addition the natural frequencies of the flexible extension, indicated by dashed lines, are present as additional peaks in the acoustic spectrum. This is consistent with the analytical predictions of [8] and findings of our previous study [10]. The fact that the shedding frequency and the second natural frequency of the structure are very close confirm the findings about the mode two shaped structural deflection from figure 6.

Conclusion

A framework to conduct DNS of flows around airfoils with flexible trailing-edge extensions was developed and the newly implemented methods validated. The setup allows to compute the hydrodynamic and acoustic field simultaneously. Initial results of a flow with $Re = 50000$ at an angle of attack of $\alpha = 4$ were presented.

Acknowledgements

The first author is grateful for the funding provided from the Faculty of Engineering and the Environment at the University of Southampton, UK.

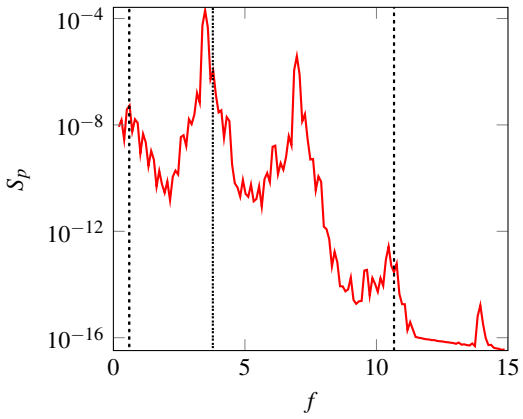

Figure 7. Spectral power density of pressure signal at a $(x,y) = (-3.322, 4.97)$ from the simulation with a flexible TE extension. This position is also highlighted in figure 5. The dashed vertical lines are the natural frequencies of the structural vibration.

References

[1] Blackstock, D., *Fundamentals of Physical Acoustics*, John Wiley & Sons, 2000.

[2] Husmeier, F., Mayer, C. and Fasel, H., Investigation of Transition of Supersonic Boundary Layers at Mach 3 Using DNS, AIAA Paper 2005-95, 2005.

[3] Jaworski, J. and Peake, N., Aerodynamic noise from a poroelastic edge with implications for the silent flight of owls, *J. Fluid Mech.*, **723**, 2013, 456–479.

[4] Jones, L., Sandberg, R. and Sandham, N., Direct numerical simulations of forced and unforced separation bubbles on an airfoil at incidence, *J. Fuid Mech.* , **602**, 2008, 175–207.

[5] Kim, J., High-order compact filters with variable cut-off wavenumber and stable boundary treatment, *Computers & Fluids*, **39**, 2010, 1168–1182.

[6] Kim, J. and Sandberg, R., Efficient parallel computing with a compact finite difference scheme, *Computers & Fluids*, **58**, 2012, 70–87.

[7] Maertens, A. P. and Weymouth, G. D., Accurate Cartesian-grid simulations of near-body flows at intermediate Reynolds numbers,*submitted to Comput. Method Appl. M.* .

[8] Manela, A., Sound generated by a vortex convected past an elastic sheet, *J. of Sound Vib.*, **330**, 2011, 416–430.

[9] Mayer, C., von Terzi, D. and Fasel, H., Direct numerical simulation of complete transition to turbulence via oblique breakdown at Mach 3, *J. Fluid Mech.*, **674**, 2011, 5–42.

[10] Schlanderer, S. and Sandberg, R., DNS of a Compliant Trailing Edge Flow, AIAA Paper 2013-2013, 2013.

[11] Thomsen, J., *Vibrations and Stability*, Springer Verlag, 2004, 2 edition.